

Technical Note

**Optical Absorbance Measurements of Opaque
Liquids by Pulsed Laser Photoacoustic Spectroscopy**

Thomas Schmid, Ulrich Panne, Reinhard Niessner, and Christoph Haisch

Anal. Chem., **2009**, 81 (6), 2403-2409 • DOI: 10.1021/ac802323t • Publication Date (Web): 17 February 2009

Downloaded from <http://pubs.acs.org> on April 3, 2009

More About This Article

Additional resources and features associated with this article are available within the HTML version:

- Supporting Information
- Access to high resolution figures
- Links to articles and content related to this article
- Copyright permission to reproduce figures and/or text from this article

[View the Full Text HTML](#)



ACS Publications
High quality. High impact.

Optical Absorbance Measurements of Opaque Liquids by Pulsed Laser Photoacoustic Spectroscopy

Thomas Schmid,[†] Ulrich Panne,[‡] Reinhard Niessner, and Christoph Haisch*

Chair for Analytical Chemistry, Technische Universität München, Marchioninistrasse 17, 81377 Munich, Germany

In many relevant industrial applications, UV–vis online process monitoring is hampered by light scattering and opacity of the samples, whereas diluted and filtered samples are rarely available. Pulsed laser photoacoustic (PA) spectroscopy allows the measurement of both high and low absorptions without any need for sample preparation. An optimized detection geometry for absorption measurements in opaque liquids is described. The proposed PA sensor was realized by using two orthogonal detectors based on piezoelectric poly(vinylidene fluoride) (PVDF). Laser-induced pressure waves were sensed perpendicularly to (side-on mode) and along the axis of the laser beam (forward mode). Pressure waves generated by a single laser pulse, optical transmission and absorption, as well as the speed of sound in liquid samples were determined simultaneously using time-resolved detection. Evaluation of the PA signal permits the determination of absorption coefficients ranging from 0.1 to 1000 cm⁻¹. The influence of absorbing or scattering compounds on the signal was investigated in dye solutions and suspensions of TiO₂ particles.

In photoacoustic (PA) or optoacoustic spectroscopy, the measurement of optical absorption is based on the conversion of optical energy into thermal energy, which results in a local expansion of the absorbing volume. With a pulsed or modulated optical excitation, the pressure waves or the expanding thermal waves are being detected. PA spectroscopy offers some distinct advantage over conventional extinction measurements: The technique is widely insensitive to light scattering in the sample, and it provides enhanced detection limits and an increased dynamic range.

The first systematic investigation of PA's suitability for absorption measurements in liquids was reported by Tam et al. in 1979¹ who applied a pulsed laser to generate the PA effect. Later, several other groups investigated the possibilities of the PA techniques

mostly with modulated rather than pulsed laser sources (see, e.g., refs 2 and 3). A direct comparison of pulsed versus modulated PA was given by Atalar.⁴ Rosencwaig did not only lay the theoretical fundamental of modulated PA measurements in liquids and solids^{5–7} but also applied pulsed PA spectroscopy to determine extremely low absorbances in liquids.⁸ Not surprisingly, most research on PA spectroscopy of liquids was focused on measurements of absorption coefficients close to the limit of detection.^{9–12} Theoretical considerations of the PA effect in highly absorbing samples are given by Terzic et al.,¹³ while the number of applications described in literature is only sparse.^{14–17} A similar approach to measure only the absorbed fraction of light for highly absorbing samples is the optothermal window technique.^{18,19}

This communication describes the construction and characterization of a photoacoustic sensor (cuvette) for optical absorption measurements in transparent and opaque liquids. The sensor principle was transferred to a flow cell which allows for online analysis of liquid samples without any need for sample preparation as described by Schmid et al.¹⁴ The emphasis of this communication lies in the optimization of the detection geometry. Therefore, two piezoelectric poly(vinylidene fluoride) (PVDF) transducers

- (2) Oda, S.; Sawada, T.; Nomura, M.; Kamada, H. *Anal. Chem.* **1979**, *51*, 686–688.
- (3) Sawada, T.; Oda, S.; Shimizu, H.; Kamada, H. *Anal. Chem.* **1979**, *51*, 688–690.
- (4) Atalar, A. *Appl. Opt.* **1980**, *19*, 3204–3210.
- (5) Rosencwaig, A. *Opt. Commun.* **1973**, *7*, 305–308.
- (6) Rosencwaig, A. *J. Appl. Phys.* **1978**, *49*, 2905–2910.
- (7) Rosencwaig, A.; Gersho, A. *J. Appl. Phys.* **1976**, *47*, 64–69.
- (8) Rosencwaig, A.; Hindley, W. T. *Appl. Opt.* **1981**, *20*, 606–609.
- (9) Hodgson, P.; Quan, M. K.; MacKenzie, A. H.; Freeborn, S. S.; Hannigan, J.; Johnston, M. E.; Greig, F.; Binnie, D. T. *Sens. Actuators, B* **1995**, *29*, 339–344.
- (10) MacKenzie, A. H.; Christion, B. G.; Hodgson, P.; Blanc, D. *Sens. Actuators, B* **1993**, *11*, 213–220.
- (11) Delgado-Vasallo, O.; Valdes, C. A.; Marin, E.; Lima, P. J. A.; Silva, D. G. M.; Sthiel, M.; Vargas, H.; Cardoso, L. *S. Meas. Sci. Technol.* **2000**, *11*, 412–417.
- (12) Quan, M. K.; MacKenzie, A. H.; Hodgson, P.; Christion, B. G. *Ultrasonics* **1994**, *32*, 181–186.
- (13) Terzic, M.; Sigrist, W. M. *J. Appl. Phys.* **1990**, *67*, 3593–3596.
- (14) Schmid, T.; Helmbrecht, C.; Haisch, C.; Panne, U.; Niessner, R. *Anal. Bioanal. Chem.* **2003**, *375*, 1130–1135.
- (15) Shen, Y.; Lu, Z.; Spiers, S.; MacKenzie, A. H.; Ashton, S. H.; Hannigan, J.; Freeborn, S. S.; Lindberg, J. *Appl. Opt.* **2000**, *39*, 4007–4012.
- (16) Hannigan, J.; Greig, F.; Freeborn, S. S.; MacKenzie, A. H. *Meas. Sci. Technol.* **1999**, *10*, 93–99.
- (17) Schlosser, U.; Schollmeyer, E.; Schmid, T.; Helmbrecht, C.; Niessner, R.; Haisch, C. *Melliand Textilberichte* **2003**, *84*, 759–762.
- (18) Defernez, M.; Tapp, S. H.; Kemsley, K. E.; Wilson, H. R. *Am. Lab.* **2002**, *34*, 34–36.
- (19) Luterotti, S.; Bicanic, D.; Pozgaj, R. *Anal. Chim. Acta* **2006**, *573*, 466–473.

* To whom correspondence should be addressed. Chair for Analytical Chemistry, Technische Universität München, Marchioninistrasse 17, 81377 Munich, Germany; phone +49 89 2180 78242; fax +49 89 2180 99 78242; e-mail Christoph.Haisch@ch.tum.de.

[†] Current address: Department of Chemistry and Applied Biosciences, ETH Zurich, 8093 Zurich, Switzerland.

[‡] Current address: Department of Chemistry, Humboldt-Universität zu Berlin, & BAM Federal Institute for Materials Research and Testing, 12489 Berlin, Germany.

(1) Tam, C. A.; Patel, N. C. K.; Kerl, J. R. *Opt. Lett.* **1979**, *4*, 81–83.

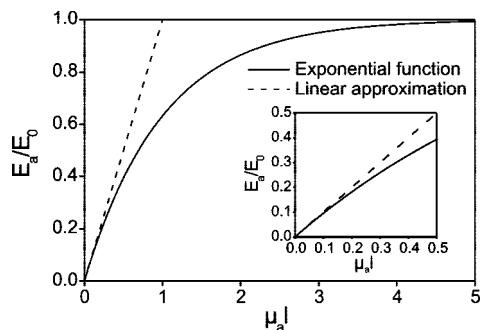


Figure 1. Normalized absorbed energy: exponential function (eq 2) and linear approximation according to eq 3.

for detection of pressure waves perpendicularly to (side-on mode) and along the laser beam direction (forward mode) were attached to the cuvette. Liquid samples within the cuvette were illuminated by short laser pulses, and the generated pressure waves were detected simultaneously in the side-on and forward modes. In this way, one has determined the optimal detection geometry for the analysis of both transparent and opaque liquids.

THEORY

Pulsed laser PA spectroscopy relies on absorption of a laser pulse (nanosecond range) and subsequent measurement of nonradiative relaxation by the detection of ultrasonic pressure pulses. The energy E_t transmitted through a sample, characterized by the optical absorption coefficient μ_a and the path length l , is given by

$$E_t = E_0 \exp(-\mu_a l) \quad (1)$$

with E_0 denoting the laser pulse energy of the incident laser beam. Because of the simple energy balance $E_0 = E_t + E_a$, the energy E_a absorbed inside the sample can be calculated through

$$E_a = E_0(1 - \exp(-\mu_a l)) \quad (2)$$

For $\mu_a l \ll 1$, eq 2 can be approximated by a Taylor series and quadratic and higher terms can be neglected. In this case, E_a can be described by a linear function:

$$E_a = E_0 \mu_a l \quad (3)$$

In Figure 1, E_a/E_0 is plotted versus $\mu_a l$. The comparison between the exponential function in eq 2 and the linear eq 3 reveals that the description of absorbed energy E_a by a linear function is only valid in the range of $\mu_a l < 0.1$. Strong saturation effects can be expected when $\mu_a l > 1$, i.e., when the optical penetration depth $\delta = 1/\mu_a$ becomes smaller than the path length l . In an opaque sample, for which $\mu_a l \gg 1$ holds true, E_a asymptotically approaches the laser pulse energy E_0 .

If the radiative relaxation processes (e.g., fluorescence and phosphorescence) or photoinduced chemical reactions can be neglected, the absorbed energy is converted solely into heat. The local warming by a laser pulse leads to a nearly adiabatic expansion of the sample matrix and the corresponding generation of an ultrasonic pressure pulse. The amplitude of the pressure

pulse Δp depends linearly on the energy absorbed inside the sample. Beyond this value, it is influenced by the thermal expansion coefficient β , the speed of sound c , the heat capacity C_p , and the path length l of the sample.²⁰

$$\Delta p \propto \frac{\beta c^2}{C_p l} E_a \quad (4)$$

Thus, Figure 1 describes also the exponential relation between Δp and μ_a which can be approximated by a linear function for small absorption coefficients. The pressure pulse propagating inside the sample can be detected by a piezoelectric sensor which is in direct contact with the sample. With dependence on the size of the laser beam and the absorbance of the sample, different acoustic waveforms are generated. The waveform depends directly on the shape of the acoustic source which in this case is the irradiated sample volume: a collimated laser beam is the source of cylindrical acoustic waves, whereas point illumination by a strongly focused radiation leads to the generation of spherical waves. According to Akhmanov et al.,²¹ the acoustic waveform depends on the radius r_b of the laser beam and on the optical penetration depth δ . Table 1 summarizes the possible relations between r_b and δ and the corresponding waveforms.²⁰

If one assumes a small, constant beam radius, the first case of a quasi-infinite illuminated area and the corresponding generation of plane waves can be neglected. This technical note describes the excitation of liquid samples inside a cuvette by either a small collimated or a focused laser beam. In this case, the problem can be simplified as described in Figure 2. If the optical penetration depth is much larger than the thickness l_c of the cuvette, the attenuation of the laser beam inside the sample can be neglected (eq 1 for $\mu_a l \ll 1$). The illuminated volume is of cylindrical shape, and hence cylindrical acoustic waves that propagate perpendicularly to the acoustic source are generated. If the illuminated volume in the case of a short optical penetration depth becomes nearly pointlike, spherical acoustic waves will be formed. When optical penetration depth is comparable to the thickness of the cuvette, both spherical and cylindrical waves are generated. These acoustic waveforms of laser-induced pressure pulses were verified previously by Schlieren photography.²²

After a certain time delay t , the generated pressure pulses reach the cuvette walls where a detector can be placed. The time delay simply depends on a distance z and the speed of sound c in the corresponding medium:

$$t = \frac{z}{c} \quad (5)$$

The transfer of acoustic energy from the sample to the detector depends on the acoustic impedance Z of the materials involved:

$$Z = \rho c \quad (6)$$

(20) Gusev, E. V.; Karabutov, A. A. *Laser Optoacoustics*; AIP Press: New York, 1991.

(21) Akhmanov, A. S.; Gusev, E. V.; Karabutov, A. A. *Infrared Phys.* **1989**, *29*, 815–838.

(22) Emmony, C. D.; Siegrist, M.; Kneubuehl, K. F. *Appl. Phys. Lett.* **1976**, *29*, 547–549.

Table 1. Acoustic Sources and Waveforms Depending on the Laser Beam Radius r_b and Optical Penetration Depth δ (According to Gusev et al²⁰)

| | acoustic source | acoustic waveform |
|-------------------|----------------------------|-------------------|
| $r_b \gg \delta$ | large/quasi-infinite area | plane wave |
| $r_b \sim \delta$ | spherical/pointlike source | spherical wave |
| $r_b \ll \delta$ | cylinder | cylindrical wave |

where ρ is the density of the material. If an acoustic wave with an amplitude p_0 reaches the interface between the two materials with the acoustic impedances Z_1 and Z_2 , the pressure p_t transmitted from medium 1 to medium 2 is given by

$$p_t = p_0 \frac{2Z_2}{Z_1 + Z_2} = p_0 t_{1,2} \quad (7)$$

with $t_{1,2}$ denoting the acoustic transmission factor. Suitable coupling materials are necessary to achieve a substantial acoustic transmission from the sample to the detector. Because of the restricted bandwidth of microphones, piezoelectric transducers (ceramics or polymer films) are preferable for the detection of laser-induced pressure waves. In the pulsed laser PA spectroscopy of liquids, piezoelectric ceramics are often used due to their high sensitivity, mechanical stability, and chemical inertness. Direct illumination of such a detector by a laser pulse results in generation of intense pressure pulses and resonant vibrations inside the ceramic; these can be detected for several microseconds, hence superposing and covering the signals generated inside the sample. Therefore, to avoid direct illumination when investigated samples are not completely opaque, piezoelectric ceramics have to be placed perpendicular to the laser beam. This is an ideal sensor geometry for detection of cylindrical waves that propagate perpendicularly to the laser beam and is often transferred to detect spherical waves in highly absorbing and opaque samples.

EXPERIMENTAL SECTION

Photoacoustic Sensor Cuvette. A conventional 1 cm glass cuvette (Hellma, Müllheim, Germany) with piezoelectric transducers placed on two sides was used for construction of the PA sensor cuvette. To detect laser-induced pressure pulses, the circular 25 μm thick and 6 mm diameter piezoelectric poly(vinylidene fluoride) (PVDF) films (Piezotech SA, Saint-Louis, France) were employed. To achieve good acoustic and electrical contact, the PVDF films were glued to the outer walls of the cuvette using a conductive epoxy (Circuit Works, Planned Products, Santa Cruz, CA), which also acts as the electrode and contact. In this way, a suitable acoustic transmission factor of 0.82 from an aqueous sample to the PVDF film was obtained. For each interface, transmission factors can be calculated according to eq 7. The product of all factors is the overall transmission factor of the detector, i.e., the system "water/coupling layers/PVDF". A more detailed description of the materials involved and the corresponding transmission factors can be found in ref 14.

Inner conductors of BNC sockets were attached to the rear of the piezoelectric films by conductive epoxy glue. In order to avoid a short circuit, both electrodes were insulated from each other by a nonconductive epoxy (UHU plus, UHU GmbH & Co. KG,

Buehl, Germany), which completely covers the upper surface of the inner electrode. The epoxy layers between the PVDF film and cuvette wall were contacted to the outer conductors of two BNC sockets. This enabled good electrical contact and shielding of the piezoelectric film. Finally, both sensors were fixed by nonconductive epoxy glue and the cuvette glued to a base plate that was integrated into an optical setup from Linos Photonics (Goettingen, Germany). Figure 3a shows the schematic setup of such a piezoelectric sensor integrated into a BNC socket; the arrangement of both sensors can be seen in Figure 3b.

Laser Setup. The Q-switched frequency-doubled Nd:YAG laser (Surelite I-10, Continuum, Santa Clara, CA) was employed for excitation of the PA signals. The laser pulses (532 nm, 6 ns, 10 Hz) were attenuated (variable attenuator, Newport, Irvine, CA), focused by a plano-convex lens ($f = 100$ mm, Linos Photonics, Goettingen, Germany), and coupled into a 550 μm quartz-quartz fiber (HCG-MO550T-10, Laser Components, Olching, Germany). At the distal end of the fiber, the laser beam was focused by a biconvex lens ($f = 30$ mm, Linos Photonics, Goettingen, Germany) at the interface between entrance window of the PA sensor cuvette and liquid sample. The cuvette, fixed inside an optomechanical setup (Linos Photonics, Goettingen, Germany), could be aligned perpendicularly to and along the laser beam direction by means of micrometer screws (see below). The PA signals were preamplified (HCA-100 M-50k-C current amplifier, Femto Messtechnik, Berlin, Germany) by a factor of 1000, recorded by a digital storage oscilloscope (TDS 540, Tektronix, Beaverton, OR) and transferred, via a GPIB IEEE 488 bus, to a personal computer. The sensor system was controlled by means of an in-house developed LabVIEW software (LabVIEW 7.1, National Instruments, Austin, TX).

Investigated Samples. In most cases (see Figures 4–8, except Figures 7b and 8b), the samples under investigation were aqueous solutions of a black textile dye (Javana, KFK, Hallendorf, Germany) with concentrations in the range of 20 mg L^{-1} to 1.34 g L^{-1} corresponding to absorption coefficients ranging from approximately 0.8 up to 50 cm^{-1} at 532 nm. In order to achieve still higher absorption coefficients up to approximately 3800 cm^{-1} (see Figure 8b), aqueous solutions of the red textile dye "Remazole Red RB" (Hoechst, Frankfurt am Main, Germany) in the range of 100 mg L^{-1} up to 50 g L^{-1} were prepared. To determine the influence of scattering particles (see Figure 7b), suspensions of 10 mg L^{-1} , 100 mg L^{-1} , 1 g L^{-1} , and 10 g L^{-1} TiO_2 (P25, Degussa, Frankfurt am Main, Germany) in water were prepared by sonification in an ultrasonic bath. Measurements of acoustic velocities (see Figure 9) were verified using solutions of 100 mg L^{-1} Javana black in water, methanol, acetone, acetonitrile, and 2-propanol. Because of the restricted solubility of the textile dye in acetone, acetonitrile, and 2-propanol, 10 mg of Javana black was dissolved in 1 mL of water and further diluted with the corresponding organic solvent.

Reference Analysis. Conventional UV–vis spectroscopy (DU 650, Beckman, Fullerton, CA) in a 1 cm glass cuvette (Hellma, Müllheim, Germany) was performed ($\lambda = 532$ nm) to determine the absorption coefficient of the textile dye solutions. To record absorbances smaller than 1, the samples were diluted; dilution factors of up to 2000 were necessary.

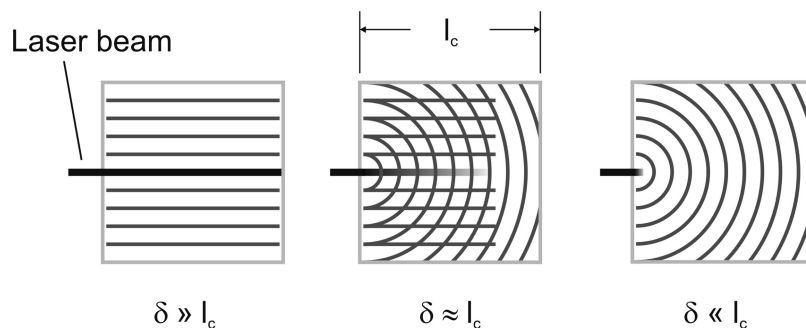


Figure 2. Schematic illustration of the relation between the optical penetration depth δ , path length of the cuvette l_c , and the acoustic waveform.

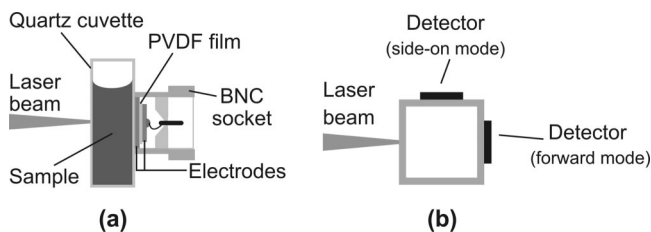


Figure 3. Photoacoustic sensor cuvette: side view revealing the setup of a piezoelectric sensor (a) and top view showing the side-on and forward mode detector (b).

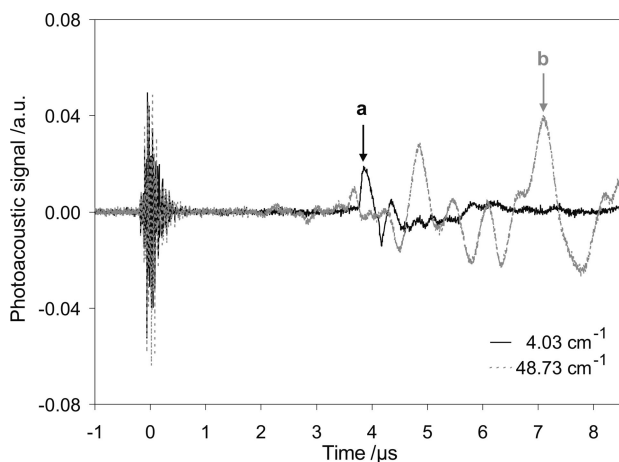


Figure 4. Characteristic PA signals for $\mu_a = 4.03 \text{ cm}^{-1}$ and $\mu_a = 48.73 \text{ cm}^{-1}$, detected perpendicularly to the laser beam (side-on mode). Signals "a" and "b" are discussed in the text.

Cuvette Alignment. With an aqueous solution of Javana black as high a concentration as 100 mg L^{-1} , PA measurements with the forward mode detector were performed. To maximize the amplitudes of the peaks in part "A" of the PA signal profile (see Figure 6), the cuvette was aligned perpendicularly to the laser beam. The alignment along the laser beam was optimized by maximizing the signal intensities in part "B" of the signal profile. In this way, the laser was focused at the interface between the entrance window and sample and aligned relative to the center of the forward mode detector.

Data Evaluation. According to eqs 2, 3, and 4, the amplitude of the PA signal depends on laser pulse energy, absorption coefficient, and various physical properties of the sample, among which the factor $\beta c^2/C_p$ depends mainly on the solvent and the sample's temperature. As only the PA signal amplitudes of aqueous samples have been evaluated, the physical properties

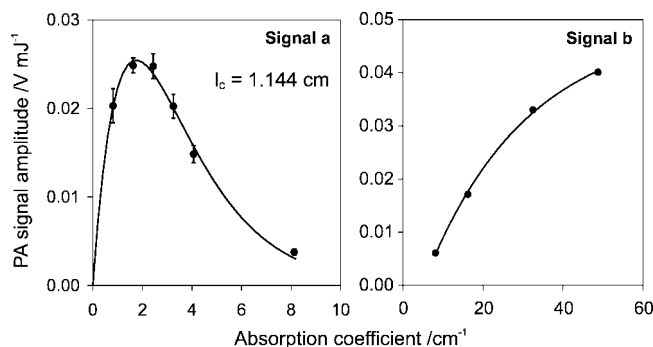


Figure 5. Maximum of signals "a" and "b" (see Figure 4) plotted versus the absorption coefficient of the sample.

of water were considered to calculate $\beta c^2/C_p$ (with $c = 1490 \text{ m s}^{-1}$).²³ Measurements at different temperatures were normalized to $25 \text{ }^\circ\text{C}$ by means of literature data as described by Adelhelm et al.²⁴ During all measurements described in this communication, the temperature varied in the range of $20\text{--}27 \text{ }^\circ\text{C}$. The acoustic velocities were determined at $25 \text{ }^\circ\text{C}$.

Average laser pulse energies were measured at the distal end of the optical fiber using a pyroelectric detector (RJ 7100, Laser Precision Corp., Utica, NY). Because the combination of preamplifier and oscilloscope used here was restricted to recording of signal amplitudes smaller than 1.8 V , it was necessary to attenuate the laser pulse energy (with a variable beam attenuator) when measuring absorption coefficients exceeding 100 cm^{-1} . The laser pulse energy varied in the range of 0.1 up to 1.2 mJ . All signal amplitudes were normalized to the laser pulse energy, i.e., $E_0 = 1 \text{ mJ}$ and are subsequently expressed in volts per millijoule.

RESULTS AND DISCUSSION

Side-On Detection. Figure 4 reveals the PA signals detected perpendicularly to the laser beam. Two characteristic signals of dye solutions with absorptions coefficients 4.03 and 48.73 cm^{-1} , respectively, are displayed. The origin of the abscissa corresponds to the instant of laser pulse generation, while the signal strongly depends upon the absorption coefficient. In both cases, simultaneously with the laser pulse, a noise signal, which does not correlate with the absorption coefficient or laser pulse

(23) Weast, C. R. *CRC Handbook of Chemistry and Physics*, 61st ed.; CRC Press, Inc.: Boca Raton, FL, 1980.

(24) Adelhelm, K.; Faubel, W.; Ache, J. H. *Fresenius J. Anal. Chem.* **1990**, *338*, 259–264.

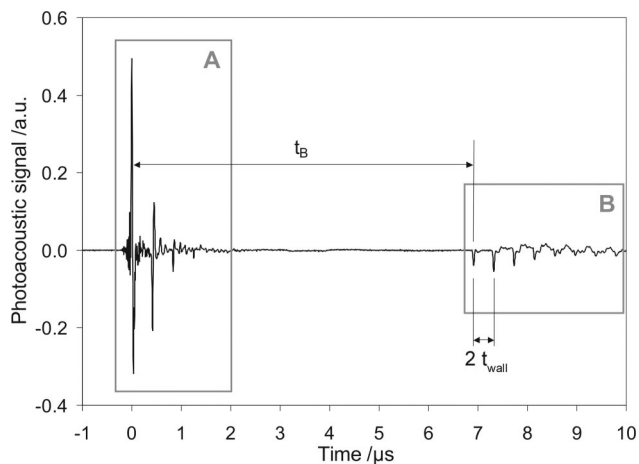


Figure 6. Typical PA forward mode signal ($\mu_a = 4.03 \text{ cm}^{-1}$). The signals “A” and “B” are discussed in the text; the time delays t_B and t_{wall} were used to determine acoustic velocities.

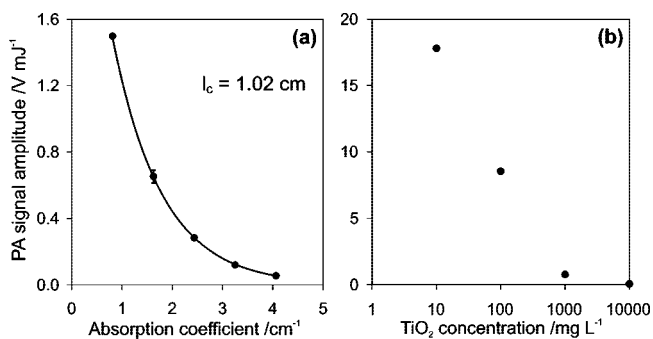


Figure 7. Maximum of signal “A” (see Figure 6, $t = 0$) plotted versus the absorption coefficient (a) and the concentration of scattering particles (b). The standard deviations are below 5% for all measurements; hence, the error bars are hidden in the data point markers.

energy, was detected. This electromagnetic interference originates from the Q-switch of the Nd:YAG laser and is detected due to an incomplete shielding of the piezosensor.

For absorption coefficients lower than approximately 10 cm^{-1} , the signal shape corresponds to that of the 4.03 cm^{-1} signal in Figure 4. The peak at $t = 3.8 \mu\text{s}$ (signal “a”), which varies with the absorption coefficient and laser pulse energy, can be explained by the photoacoustic effect (see below). According to eq 5, the time delay of $3.8 \mu\text{s}$ corresponds to a distance of 5.7 mm in water and the acoustic velocity of which is 1490 m s^{-1} . This, in turn, corresponds approximately to the distance $l_c/2$ between the piezoelectric detector and the center of cuvette, the location where a cylindrical acoustic wave is generated in weakly absorbing samples. Deviations from $l_c/2$ have two reasons: First, the laser beam was aligned on the center of the forward mode sensor by maximizing the signal intensity. Thus, because of construction tolerances, the laser beam was not exactly in the center of the cuvette. Second, the time needed for the pressure wave to pass through the 1 mm cuvette wall has to be taken into account.

The normalized maximum of this pressure pulse plotted versus the absorption coefficient of the sample is shown in Figure 5a. The maximum at $\mu_a = 3.5 \text{ cm}^{-1}$ can be explained by combining

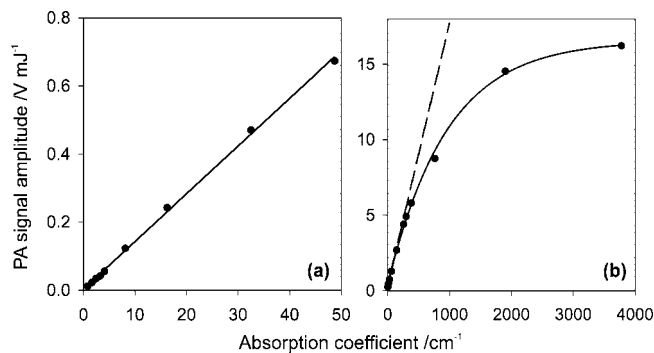


Figure 8. Calibration functions for signal “B” (see Figure 6, $t = 7.3 \mu\text{s}$): linear range (a) and exponential function (b). All standard deviations are below 5% for all measurements; hence, the error bars are hidden in the data point markers.

eqs 3 and 4; hence, the PA signal amplitude can be described by a simplified formula:

$$\Delta p = CE\mu_a \quad (8)$$

where C is a constant and E is the excitation energy at the site of the acoustic source, which in this case is approximately the center of the cuvette. The optical penetration depth is in the range of the cuvette dimensions. Thus, the laser pulse energy is attenuated due to absorption according to eq 1 and reaches

$$E = E_0 \exp(-\mu_a l_c / 2) \quad (9)$$

at the source of the pressure pulse. Combination of eqs 8 and 9 leads to a function with a maximum at $\mu_a = 2/l_c$:

$$\Delta p = C\mu_a E_0 \exp(-\mu_a l_c / 2) \quad (10)$$

Fitting this equation to the data presented in Figure 5 reveals a value of $l_c = 1.144 \text{ cm}$, which is in reasonable agreement with the expected value of 1 cm, considering the limitations for this calculation stated above.

For low absorption coefficients, the amplitude of the generated cylindrical pressure wave depends linearly on μ_a ; such a case of PA trace analysis with the perpendicular detection was described in the literature previously.⁹ As the optical penetration depth becomes comparable to the dimensions of the cuvette, the second term becomes important, describing an exponential attenuation with increasing μ_a . Both effects lead to a discontinuous calibration function with a local maximum that cannot be used for determination of the absorption coefficients based on the evaluation of the PA signals. Thus, PA absorption measurements by detection of cylindrical waves in a direction perpendicular to the laser beam are restricted only to trace analysis. It can be concluded, that signal “a” is a cylindrical wave propagating perpendicularly to the laser beam, which is generated by the photoacoustic effect in the center of the cuvette.

In the range of approximately $\mu_a > 10 \text{ cm}^{-1}$ or $\delta < l_c$, a significant change in the signal shape was observed. According to Figure 2, this can be explained by a change in the acoustic waveform: for $\delta \ll l_c$, only spherical acoustic waves are generated by the photoacoustic effect. All peaks in the signal

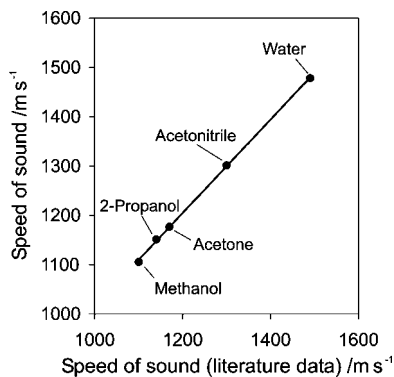


Figure 9. Determination of the speed of sound by PA measurements: comparison of experimental and literature data.

profile correlate with the absorption coefficient and laser pulse energy and correspond to various phase fronts and reflections of a laser-induced shock wave. In Figure 5b, the most intense pressure pulse at $t = 7.1 \mu\text{s}$ is plotted versus the absorption coefficient of the sample. As depicted in Figure 2c, the spherical waves are generated very close to the entrance window of the cuvette; hence, the penetration depth of the laser beam can be neglected. According to eq 2, an exponential function was fitted to the measured data. By a nonlinear curve fitting, the path length l was determined to be 0.039 cm ($R^2 = 0.999$; number of measurements, $n = 4$; number of repetitions per measurement, $m = 3$). In conventional, transmission based optical absorption measurements, i.e., UV–vis spectroscopy, the path length l corresponds to the thickness of the cuvette l_c . Here, the PA signal reflects obviously only a small part of the sample. With a characteristic path length of 0.39 mm , the dynamic range is enlarged by a factor of approximately 25 with respect to UV–vis spectroscopy in a 1 cm cuvette. According to Figure 1 and eq 4, the PA signal amplitude can be described by a linear function in the range of $\mu_a l < 0.1$. In this case, absorption coefficients smaller than 7.4 cm^{-1} fulfill this condition. Thus, all measurement values revealed in Figure 5b are located in the nonlinear saturation regime.

Forward Mode Detection. Figure 6 displays a typical signal detected in a forward mode ($\mu_a = 4.03 \text{ cm}^{-1}$). The signal profile consists of two parts: part “A” from $t = 0$ to $t = 2 \mu\text{s}$ and part “B” from $t = 7 \mu\text{s}$ to $t = 10 \mu\text{s}$. The signal detected at $t = 0$ correlates with absorption coefficient and laser pulse energy. This laser-induced pressure wave is generated inside the conductive epoxy electrode of the piezosensor by the transmitted part of the excitation energy and is detected therefore simultaneously with the laser pulse. At time delays of 420 ns , additional pressure pulses were detected; they can be explained by reflections of the first signal within the cuvette’s wall and at the glass/air interface. Thus, 420 ns is 2 times the traveling time of a pressure pulse through the cuvette wall, i.e., $2t_{\text{wall}}$. Taking into account the 1 mm thickness of the cuvette wall, the corresponding speed of the sound is 4760 m s^{-1} (according to ref 23). This value is in the range typical for acoustic velocities of different glasses. The signals in part “A” are overlaid by an electromagnetic interference generated by the Q-switch of the Nd:YAG laser.

In Figure 7a, the maximum of the signal at $t = 0$ is plotted versus the absorption coefficient of the sample. The signal is generated by the transmitted part of the laser pulse; hence, the exponential decay can be explained by eq 1. The nonlinear curve fitting ($R^2 = 0.9998$, $n = 5$, $m = 3$) reveals a path length of $l = 1.02 \text{ cm}$; this value is in a good agreement with the thickness of the cuvette, i.e., $l_c = 1 \text{ cm}$. Contrary to PA spectroscopy, in conventional transmission measurements, both light absorption and scattering lead to an alteration of the signal. In Figure 7b, the signal maxima at $t = 0$ are plotted versus the concentration of scattering particles in aqueous TiO_2 suspensions. As expected, the signal intensity decreases as the particle concentration increases. Thus, it can be concluded that with the cuvette presented here, both PA and conventional transmission measurements can be performed simultaneously.

Part “B” of the signal profile starts at $t = 6.9 \mu\text{s}$. When the traveling time of the pressure pulse through the 1 mm thick cuvette wall (approximately 200 ns) is subtracted from this value, eq 5 gives a distance of 1 cm based on $c = 1490 \text{ m s}^{-1}$, the speed of sound in water. Thus, the pressure waves generated at the interface between the aqueous sample and the cuvette wall are detected by the forward mode detector after propagating along the 1 cm path length of the cuvette. The timing of the signals in part “B” was constant over the whole absorption range under investigation, i.e., 0.8 cm^{-1} up to 3780 cm^{-1} . Therefore, we can conclude that the acoustic waveform detected by the forward mode sensor was constant. As revealed by Figure 2 in the case of moderate and high absorptions, spherical waves are generated at the irradiated sample surface and can be detected both in the side-on and forward mode, whereas the phase fronts of cylindrical waves do not affect the forward mode sensor. After propagation through the 1 cm cuvette, the phase fronts of the spherical waves are relatively large compared to the 6 mm piezosensor. The quasi-plane waves are therefore detected, which leads to the occurrence of sharper peaks in the signal profile when compared to side-on detection.

All peaks in part “B” of the signal vary with the absorption coefficient and the laser pulse energy as predicted by the theory of the PA effect. For calibration, the absolute values of the signal minima were evaluated. In all cases, the peak at $t = 7.3 \mu\text{s}$ had the highest amplitude. Figure 8a shows the absolute value of its minimum plotted versus the absorption coefficient of the sample. The calibration function is linear over the whole range from 0.8 cm^{-1} up to 50 cm^{-1} ($R^2 = 0.9987$, $n = 9$, $m = 3$). The IUPAC 3 s_B criterion resulted in a detection limit of 0.12 cm^{-1} . The slope of the line of best fit that corresponds to the sensitivity of the sensor was $0.014 \text{ cm V mJ}^{-1}$. For a more detailed characterization of the dynamic range, the calibration set was expanded to include coefficients up to 3780 cm^{-1} . According to eq 2, an exponential function was fitted to the measurement values (see Figure 8b). The nonlinear curve fitting resulted in a path length of $l = 9 \mu\text{m}$. A comparison of the characteristic path lengths reveals that the dynamic range in PA forward mode measurements is expanded by a factor of 1100 with respect to UV–vis measurements in a 1 cm cuvette and a factor of 40 compared to PA measurements in the side-on mode. In this case, the PA signal amplitude can be approximated by a linear function

in the range of $\mu_a < 110 \text{ cm}^{-1}$, i.e., $\mu_a l < 0.1$; in Figure 8b, the linear approximation is given as a dashed line. For $\mu_a > 110 \text{ cm}^{-1}$, a nonlinear calibration function can be applied. Saturation effects restrict the measurement range in this case to $\mu_a < 1100 \text{ cm}^{-1}$, i.e., $\delta < 1$. The origin of this saturation remains to be investigated in future work. As the PA signal reflects only the absorbed fraction of the laser pulse energy, no signal in part "B" was detected when TiO_2 suspensions were irradiated inside the cuvette.

Determination of Acoustic Velocities. Absorption coefficients or optical transmissions, respectively, can be determined by evaluating the amplitude of detected pressure pulses. Additionally, the transit time of the pressure reflects the properties of the sample under investigation. As stated above, the time delay between both parts of the forward mode signal profile (see Figure 6) corresponds to the traveling time of pressure waves along the path length of the cuvette. Since the cuvette path length is constant ($l_c = 1 \text{ cm}$), acoustic velocities can be determined from eq 5; this was verified by using textile dye solutions in different solvents with known acoustic velocities as described in the Experimental Section and performing PA measurements.

The time delay t_B between the signal at $t = 0$ (part "A") and the first signal in part "B" of the PA signal profile was recorded to determine the acoustic velocities (see Figure 6). According to eq 5, the speed of sound c_{Exp} was calculated from

$$c_{\text{Exp}} = \frac{l_c}{t_B - t_{\text{wall}}} \quad (11)$$

where t_{wall} is the time needed for the pressure pulse to transit the cuvette wall and reach the detector. This quantity was determined experimentally by evaluating the multiple reflections of pressure waves within the cuvette wall (see Figure 6); a mean value for $t_{\text{wall}} = 201 \text{ ns}$ with a standard deviation of 6 ns was measured. As expected, t_B varied due to different acoustic velocities when the solvent was changed, whereas t_{wall} remained constant. Measured values are plotted versus corresponding

reference data²³ in Figure 9. For each experimentally determined acoustic velocity, deviations range from 0.1 to 1%. Figure 9 illustrates the linear relation ($R^2 = 0.9996$, $n = 5$, $m = 3$) between both sets of data and confirms a good agreement between measured values and literature data.

CONCLUSIONS

The detection scheme for PA signals of highly absorbing liquids presented here significantly expands the dynamic range for such systems to a maximum value of $\mu_a = 1100 \text{ cm}^{-1}$. We are confident that this type of optical arrangement can help to foster the application of photoacoustics to characterize optical properties of nearly opaque and scattering liquids. The realization of the flow cells for online analysis based on the same detection scheme has already been demonstrated by our group.¹⁴ Combining the proposed setup with steadily emerging modern tunable laser sources such as optical parametrical oscillators (OPO) or pulsed laser diodes⁹ allows for the construction of analytical systems suitable for routine industrial application. Pulsed laser PA spectroscopy enables simultaneous determination of optical absorption, extinction, and speed of sound. It can be applied not only to liquids, like textile dyes, but also to viscose media like gels and paste. Because of the different acoustical properties of such materials, the system needs to be calibrated specifically for each material. A typical task could be the quantification of the sugar content in molasses, for instance, or the analysis of other semiviscous foodstuff.

ACKNOWLEDGMENT

The authors acknowledge the financial support by Deutsche Forschungsgemeinschaft (DFG) and a grant by Max-Buchner-Forschungsstiftung awarded to Thomas Schmid.

Received for review November 4, 2008. Accepted January 26, 2009.

AC802323T